Supplementary Information

Transient Polymer Electronics Enabled by Grafting of Oligo-3-hexylthiophenes onto Polycaprolactone

Eddie Wai Chi Chan[a,b], Xin Sun[a,b], Yuhka Uda[a,b], Bicheng Zhu[a,b], David Barker[a,b], Jadranka Travas-Sejdic[a,b]*

[a]Centre for Innovative Materials for Health, School of Chemical Sciences, The University of Auckland - Waipapa Taumata Rau, 23 Symonds Street, Auckland, 1023, New Zealand

[b]MacDiarmid Institute for Advanced Materials and Nanotechnology, Kelburn Parade, Wellington, 6140, New Zealand

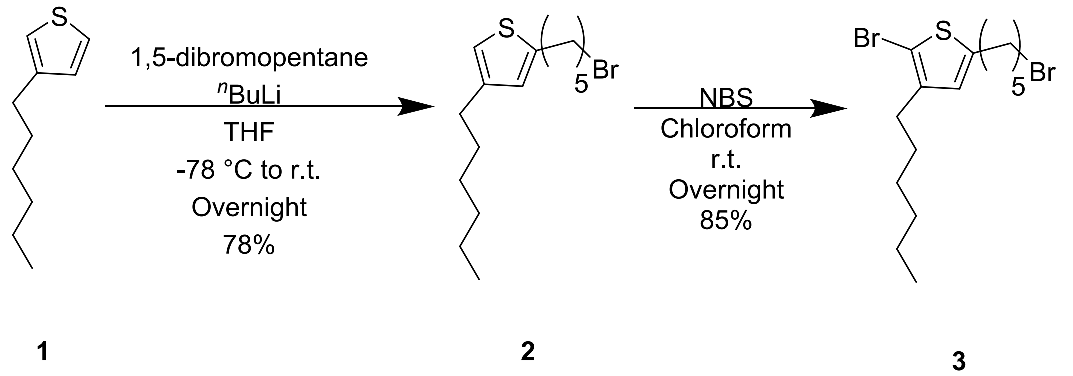

Scheme S1: Synthesis of capping group 2-bromo-5-(bromomethyl)-3-hexylthiophene **3**.

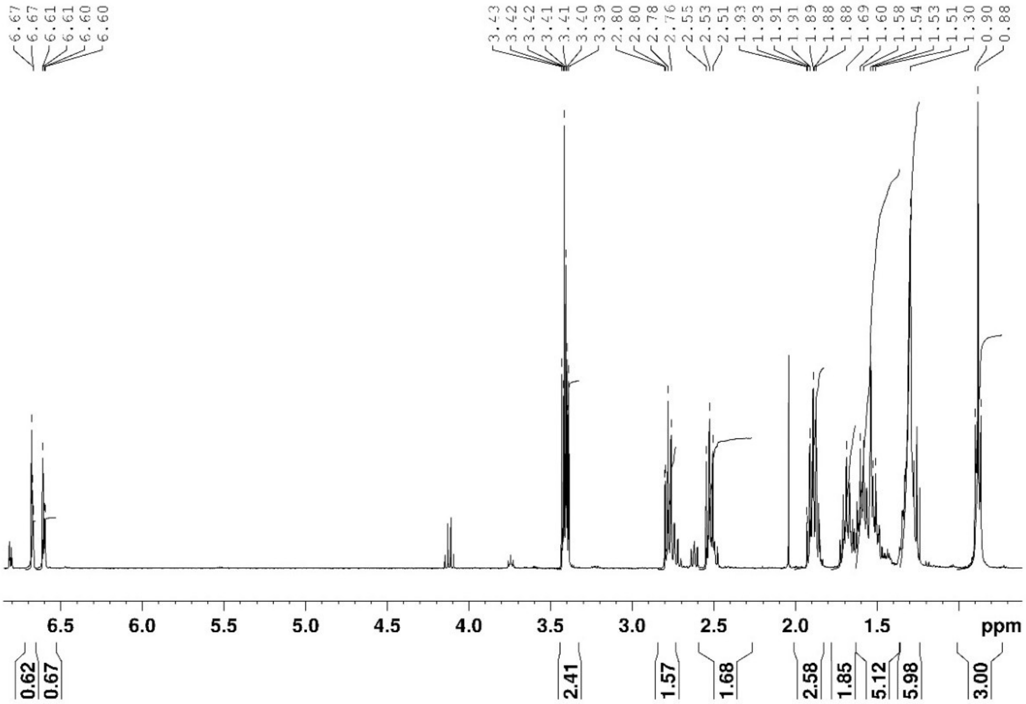

Figure S1: ^{1}H NMR spectra of 2-(5-bromopentyl)-4-hexylthiophene **2**.

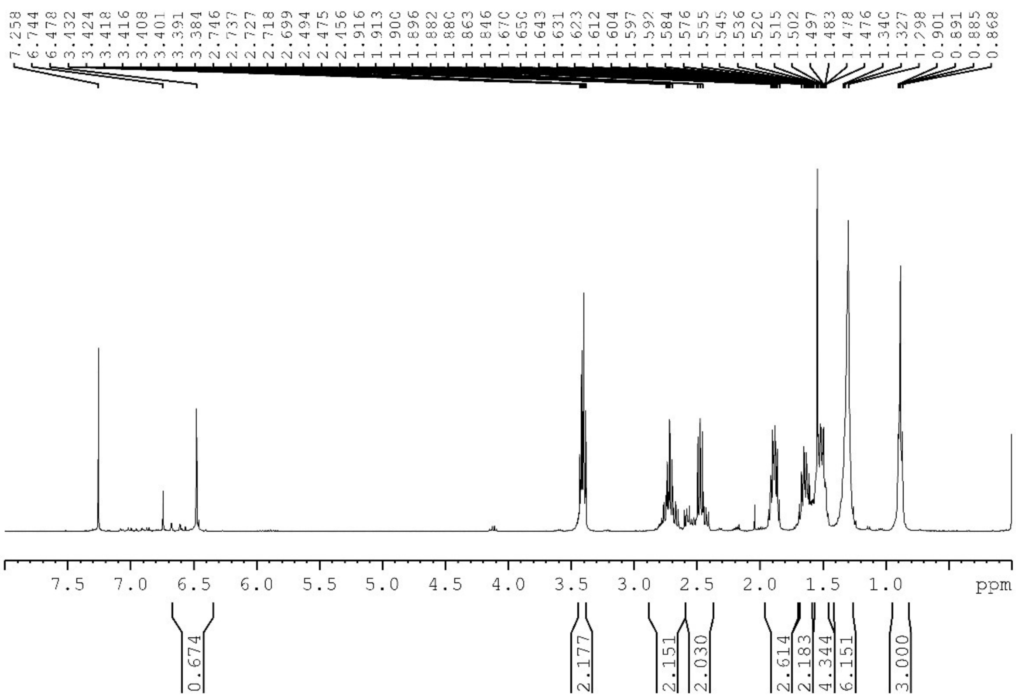

Figure S2: ^{1}H NMR spectra of 2-bromo-5-(bromomethyl)-3-hexylthiophene **3**.

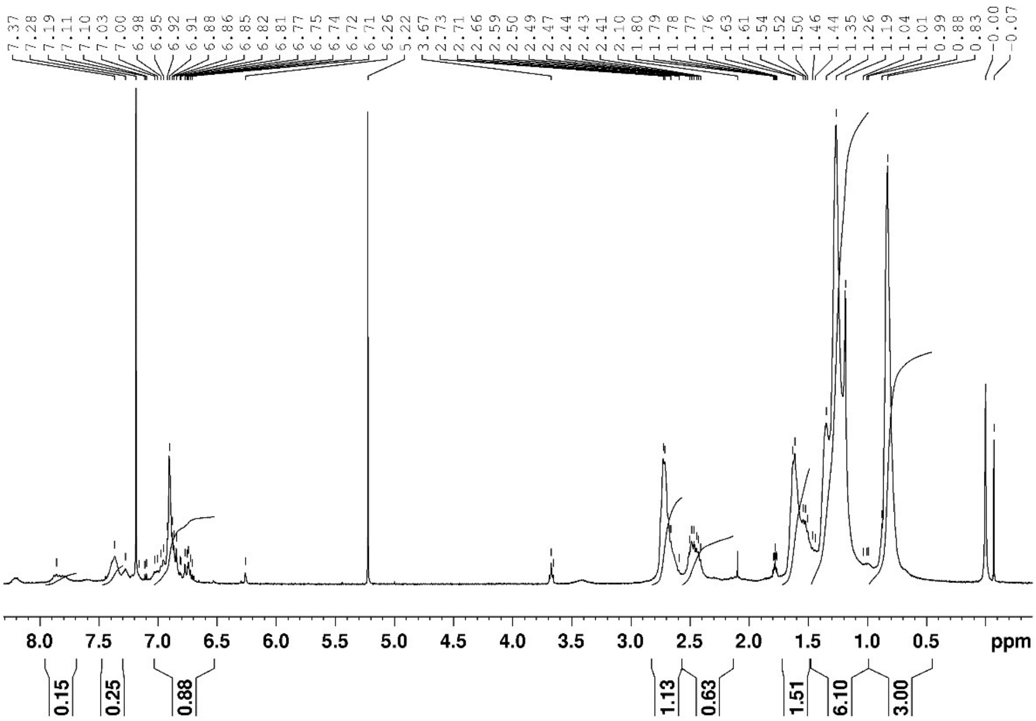

Figure S3: [1]H NMR spectra of O3HT-**15**.

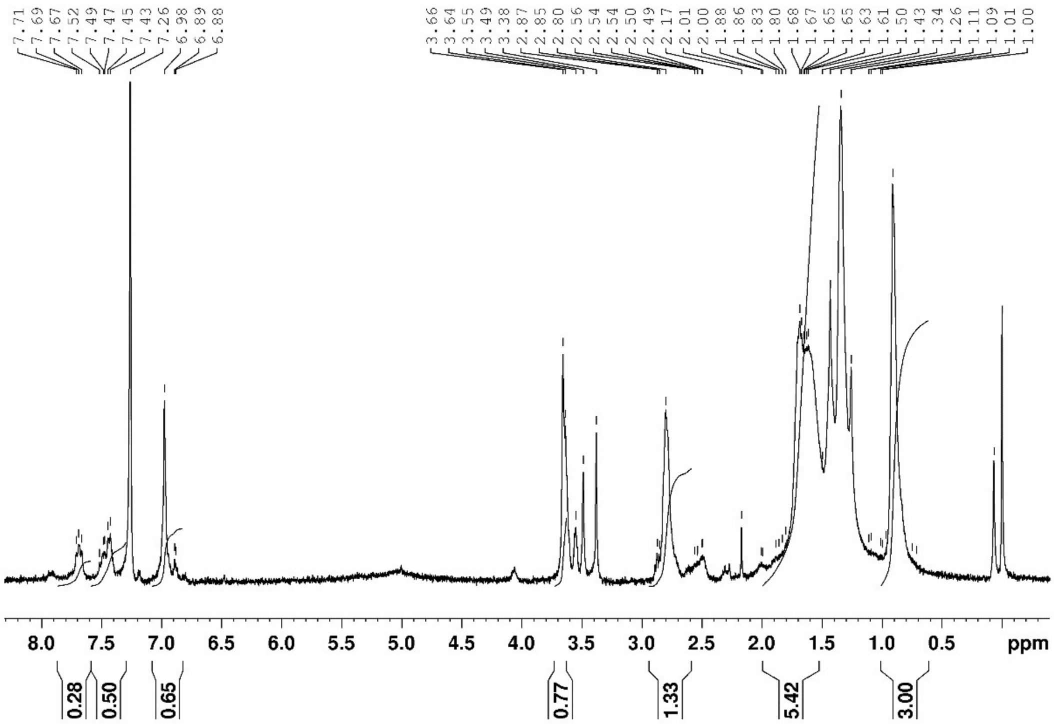

Figure S4: [1]H NMR spectra of O3HT-**30**.

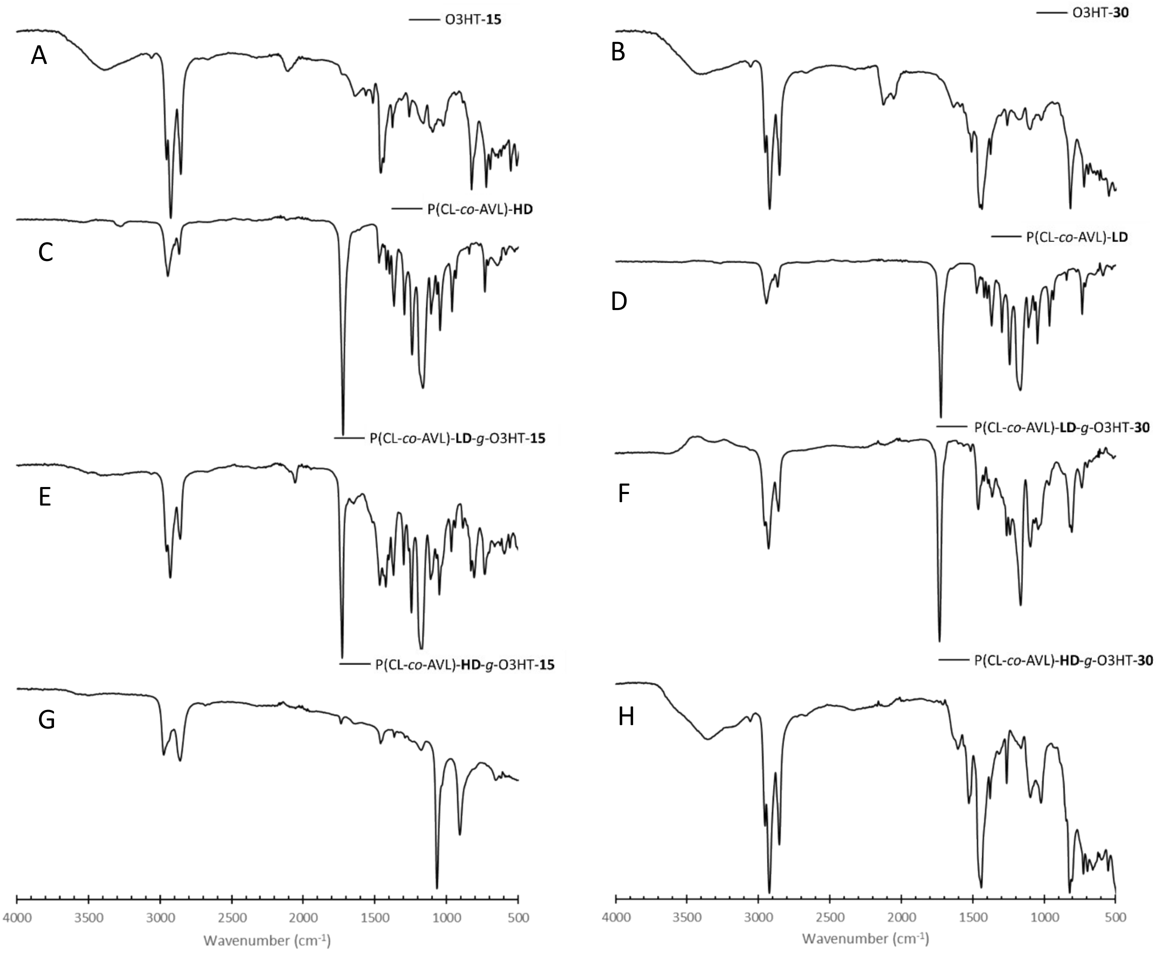

Figure S5: Normalized FT-IR spectra of O3HT-**15** (A), O3HT-**30** (B), P(CL-*co*-AVL)-**LD** (C), P(CL-*co*-AVL)-**HD** (D), P(CL-*co*-AVL)-**LD**-*g*-O3HT-**15** (E), P(CL-*co*-AVL)-**HD**-*g*-O3HT-**15** (F), P(CL-*co*-AVL)-**LD**-*g*-O3HT-**30** (G) and P(CL-*co*-AVL)-**HD**-*g*-O3HT-**30** (H).

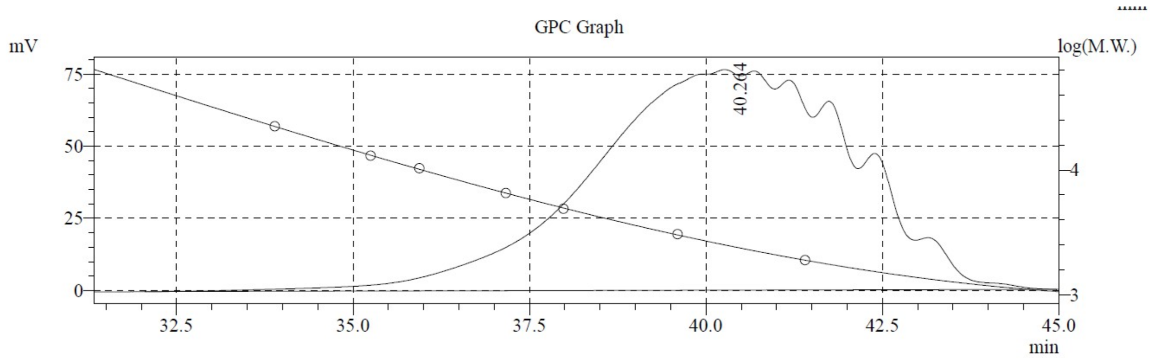

Figure S6: GPC trace of O3HT-**15**

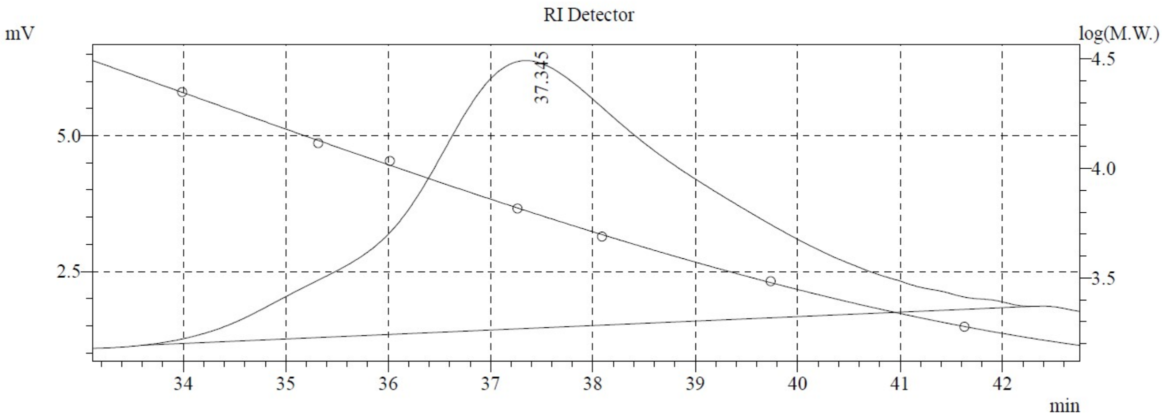

Figure S7: GPC trace of O3HT-30

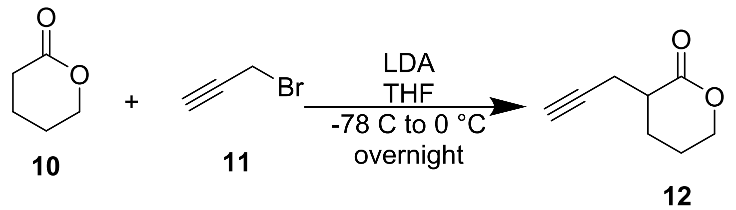

Scheme S2: Synthesis of 3-(prop-2-yn-1-yl)tetrahydro-2H-pyran-2-one **12** (alkyne-valerolactone).

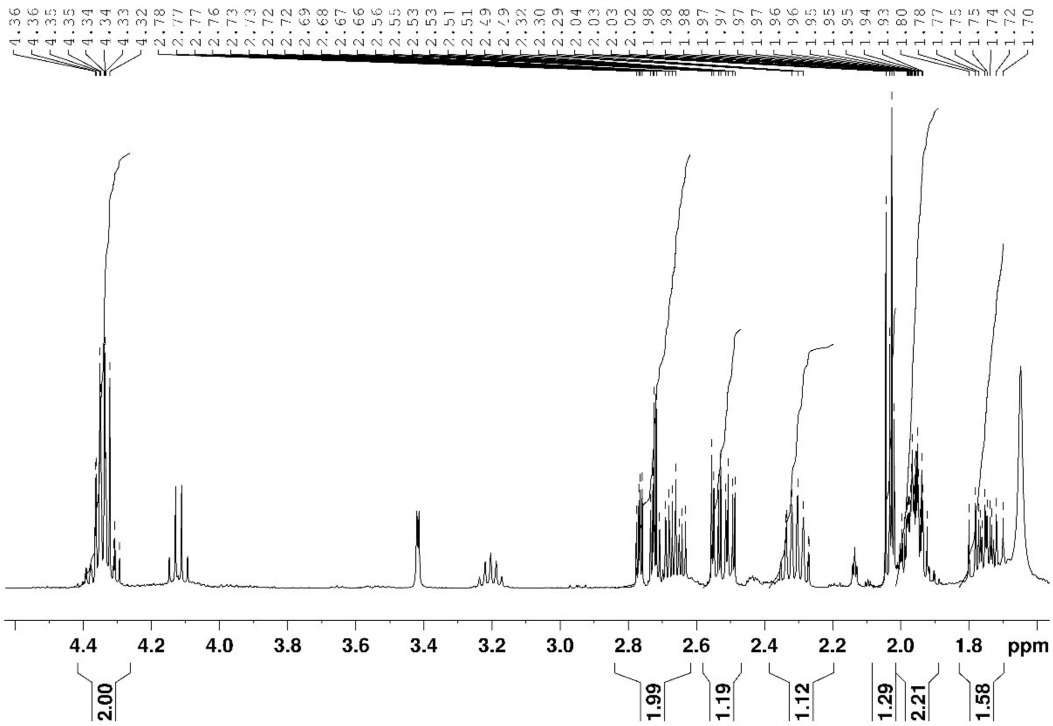

Figure S8: [1]H NMR spectra of alkyne-valerolactone **12**.

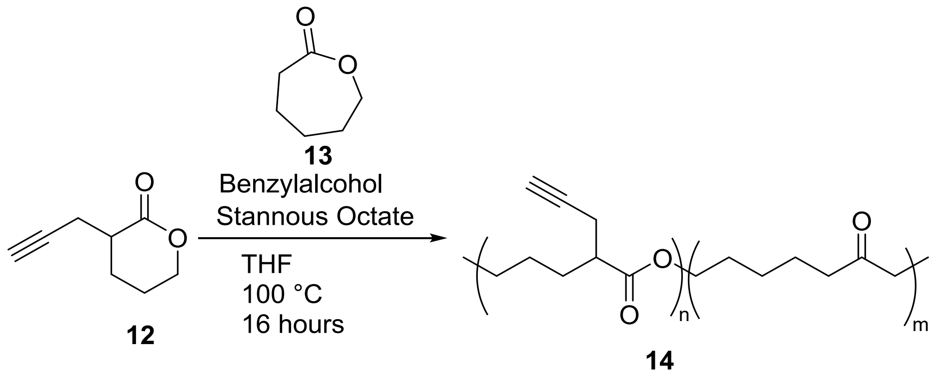

Scheme S3: Synthesis of P(CL-*co*-AVL) **14**.

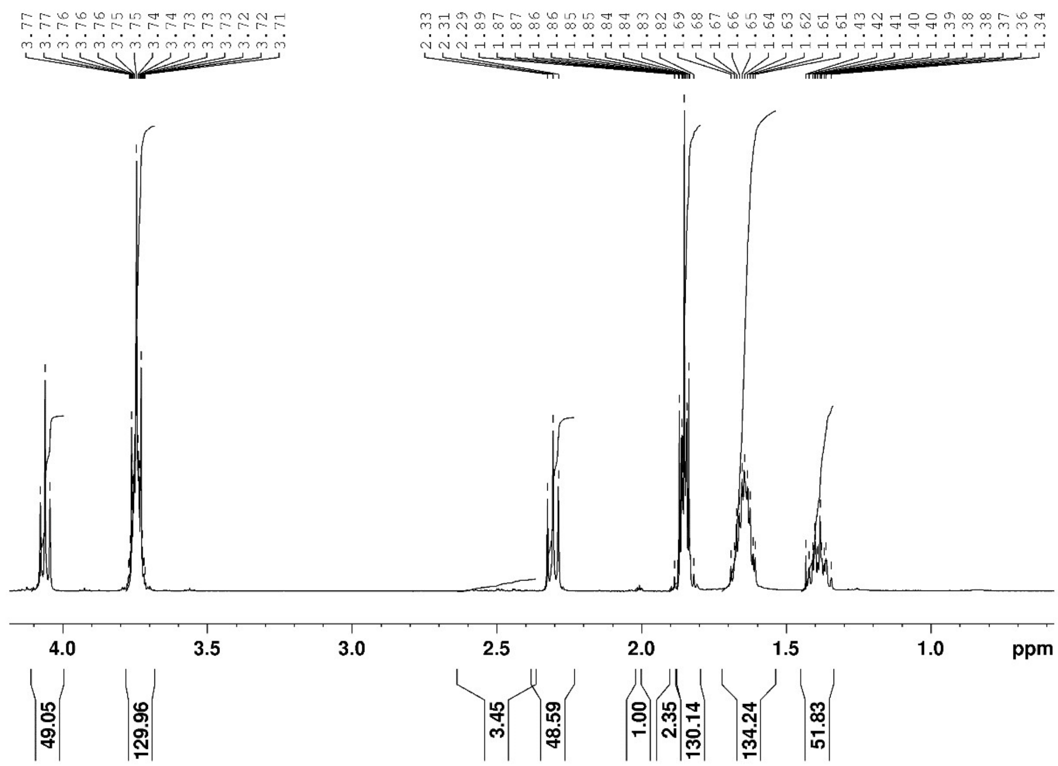

Figure S9: ^{1}H NMR spectra P(CL-*co*-AVL)-**LD**.

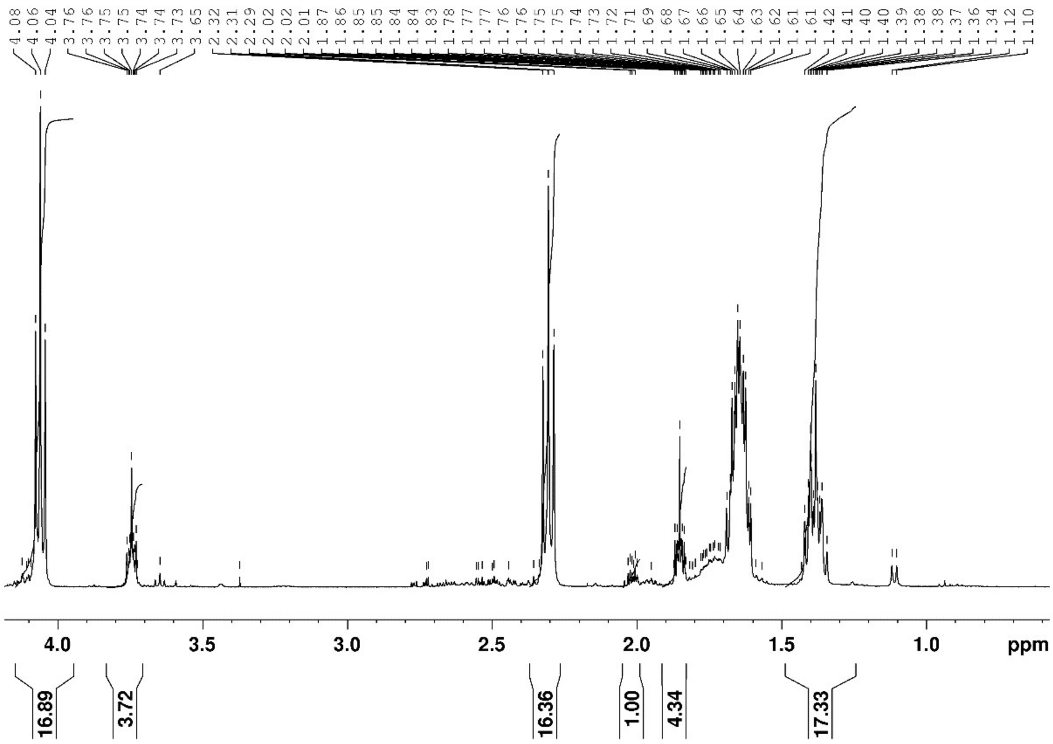

Figure S10: ^{1}H NMR spectra of P(CL-*co*-AVL)-**HD**.

Table S1: Molecular weight determination of P(CL-*co*-AVL) using GPC analysis.

Polymer	M_n (Da)	M_w (Da)	M_z (Da)	Đ	Length (mers)
P(CL-*co*-AVL)-**LD**	30640	38685	45999	1.26	340
P(CL-*co*-AVL)-**HD**	8631	11405	14695	1.32	103

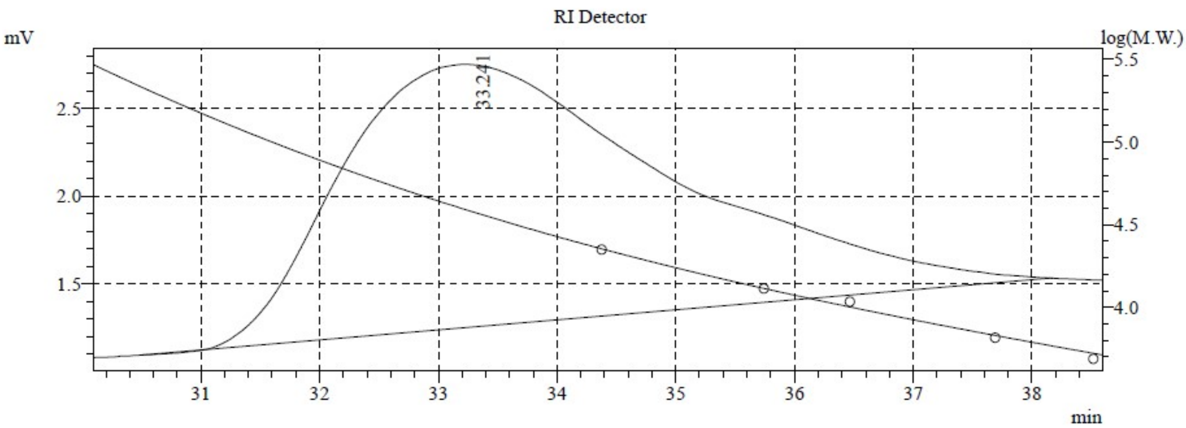

Figure S11: GPC trace of P(CL-*co*-AVL)-**LD**.

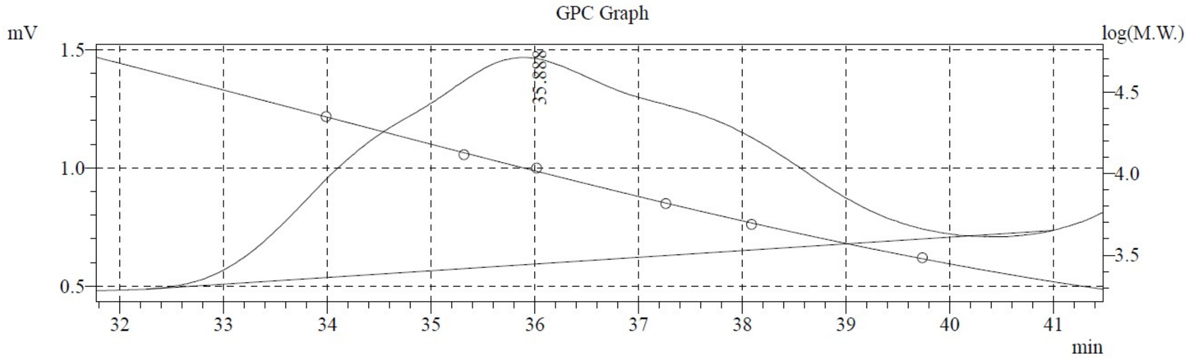

Figure S12: GPC trace of P(CL-*co*-AVL)-**HD**.

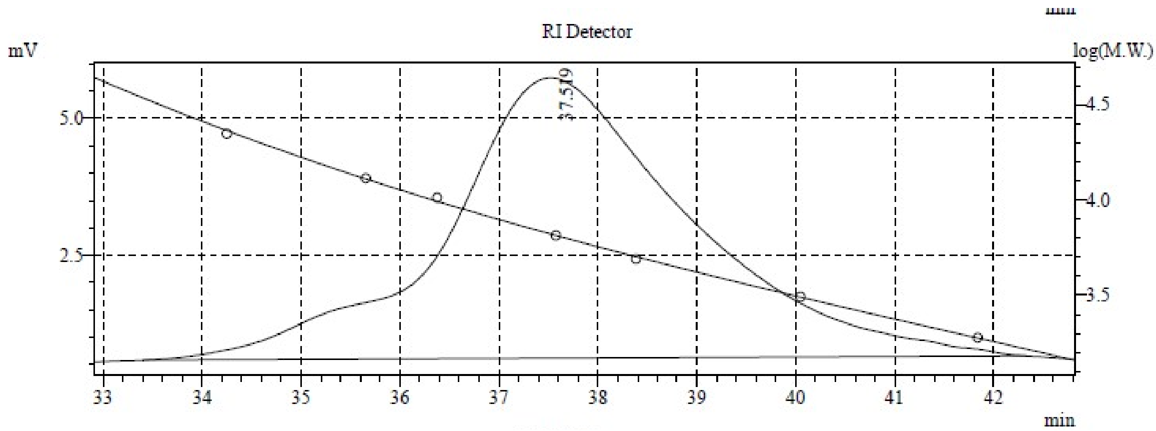

Figure S13: GPC trace of P(CL-*co*-AVL)-**LD**-*g*-O3HT-**15**.

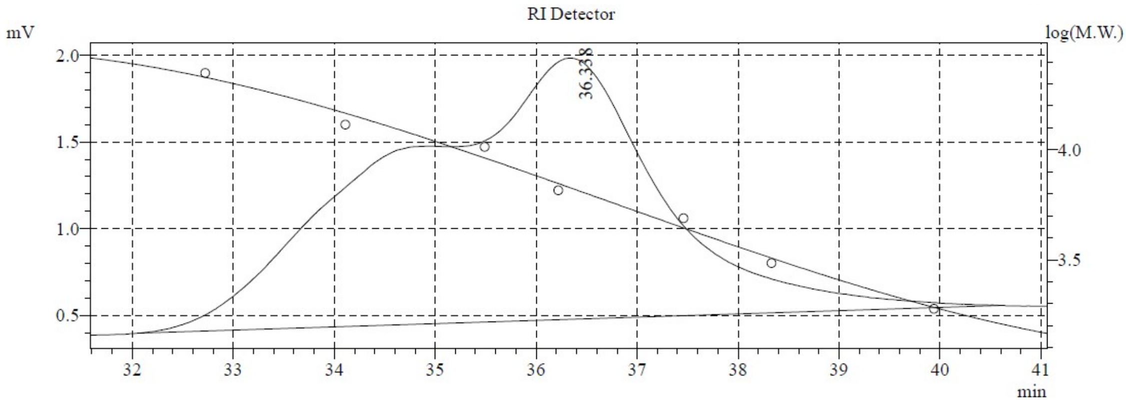

Figure S14: GPC trace of P(CL-*co*-AVL)-**HD**-*g*-O3HT-**15**.

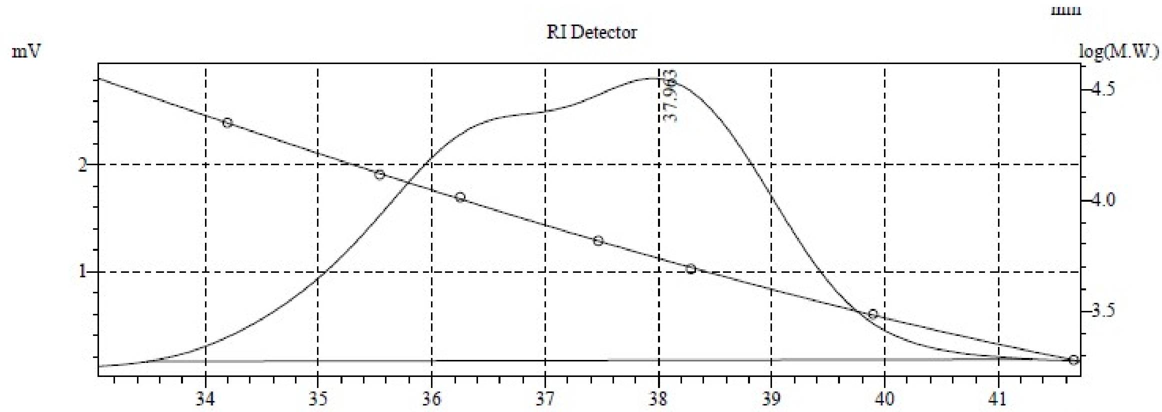

Figure S15: GPC trace of P(CL-*co*-AVL)-**LD**-*g*-O3HT-**30**.

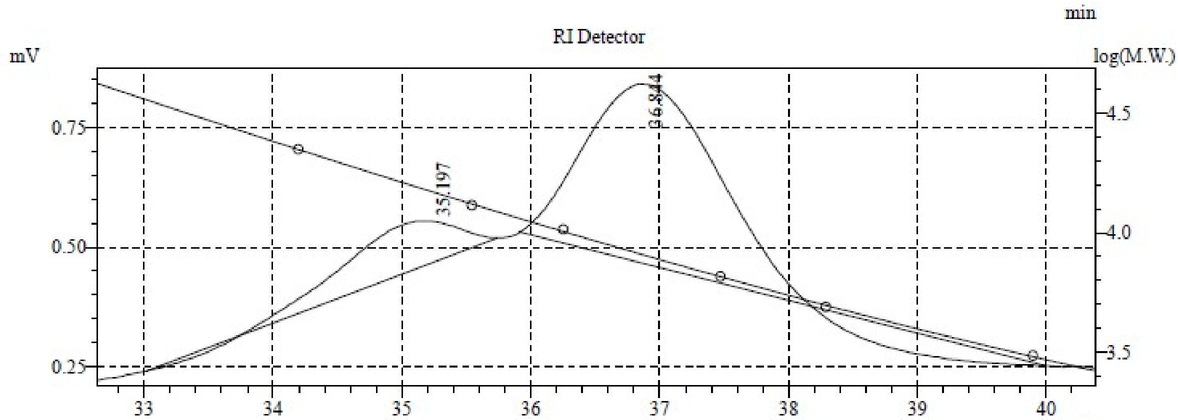

Figure S16: GPC trace of P(CL-*co*-AVL)-**HD**-*g*-O3HT-**30**.

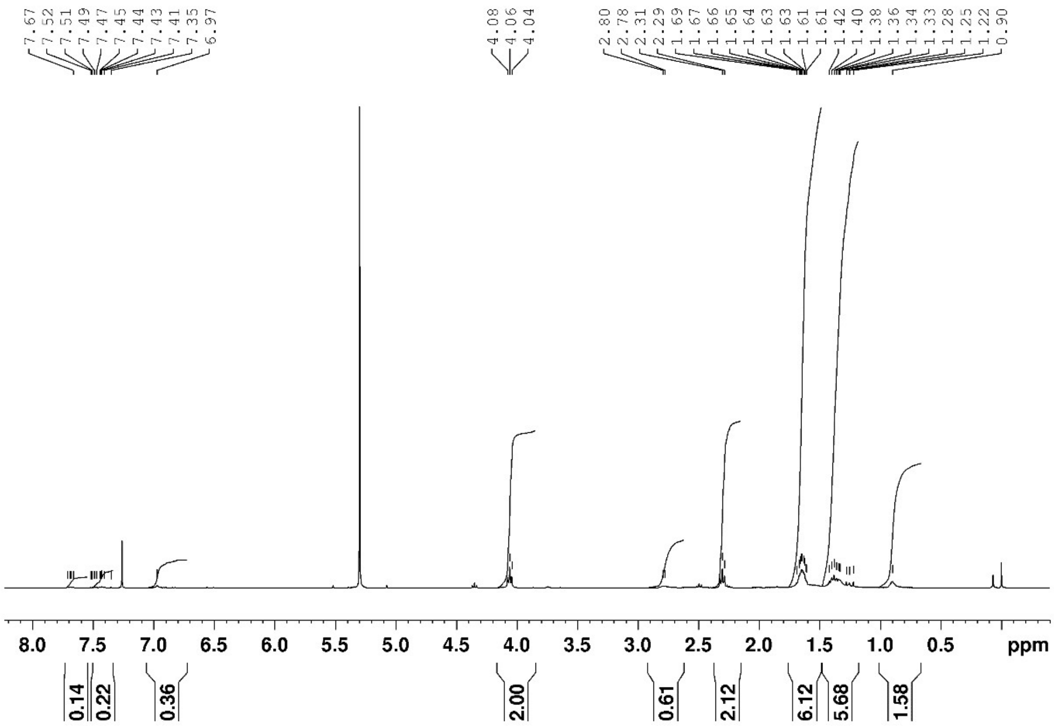

Figure S17: ^{1}H NMR spectra of P(CL-*co*-AVL)-**LD**-*g*-O3HT-**15**.

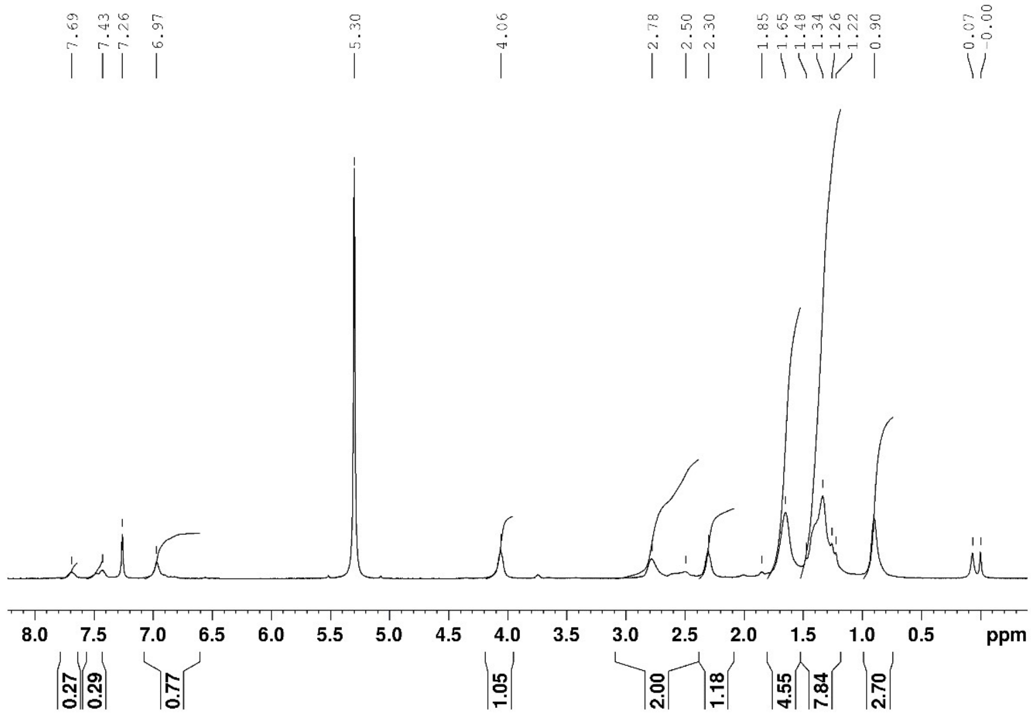

Figure S18: ^{1}H NMR spectra of P(CL-*co*-AVL)-**HD**-*g*-O3HT-**15**.

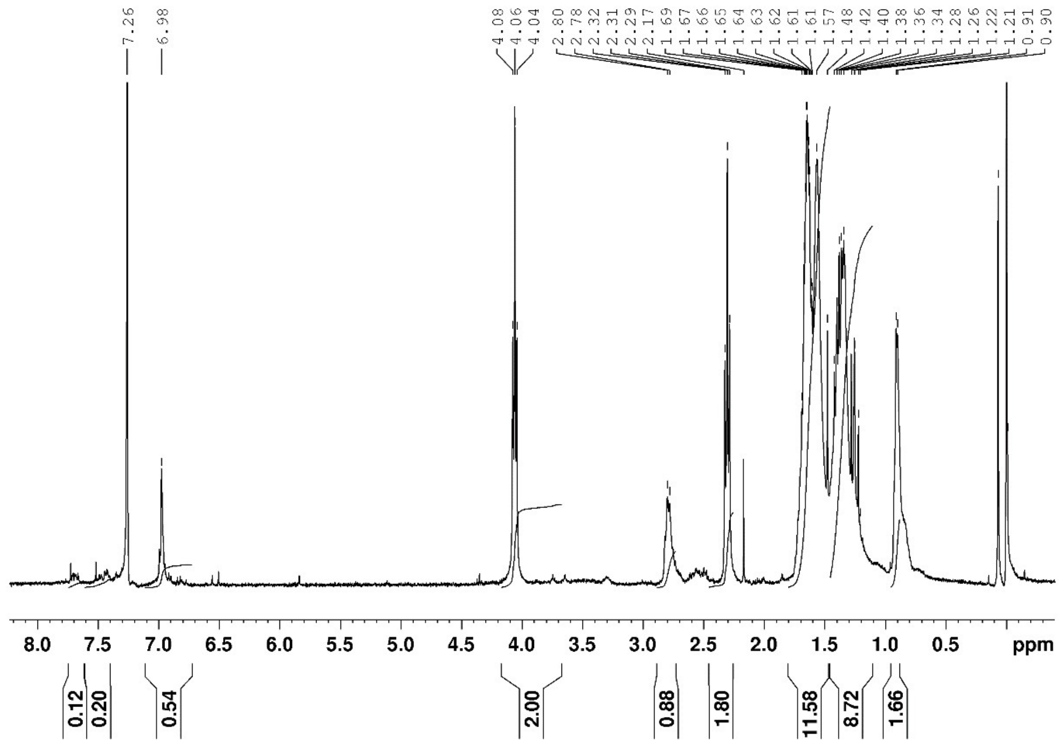

Figure S19: ^{1}H NMR spectra of P(CL-*co*-AVL)-**LD**-*g*-O3HT-**30**.

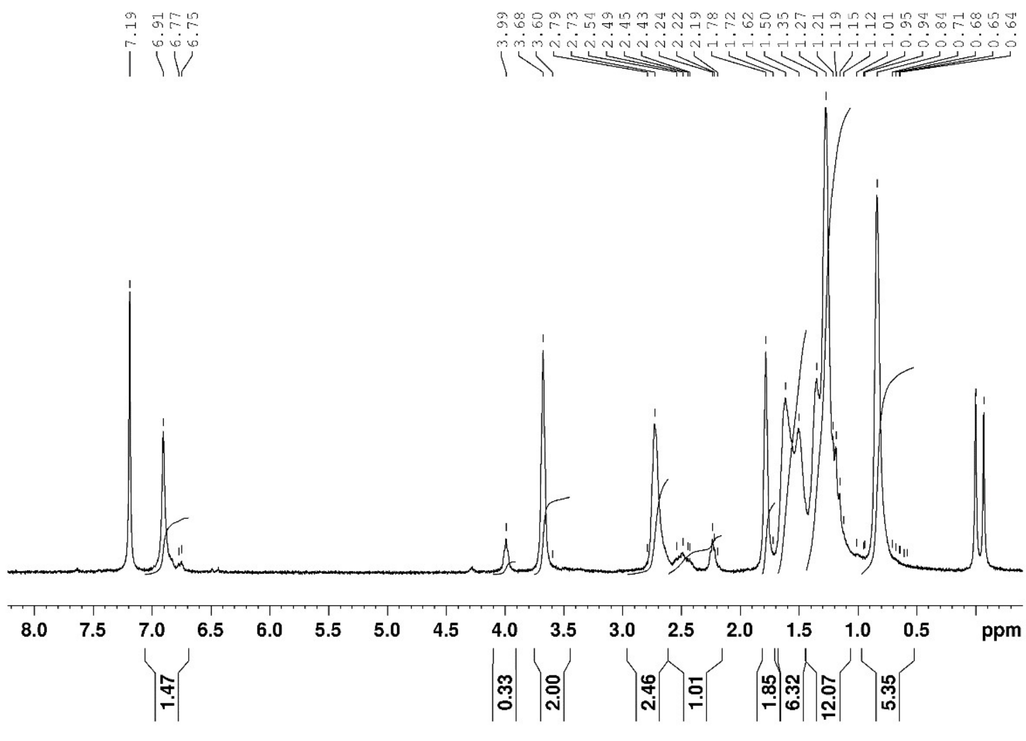

Figure S20: ^{1}H NMR spectra of P(CL-*co*-AVL)-**HD**-*g*-O3HT-**30**.

Table S2: Conductivity (measured by 4-point probe method) and film thicknesses of the grafted P(CL-*co*-AVL)-*g*-O3HTs films on glass substrates (n≥3).

Sample	**Film thickness (µm)**	**Conductivity (mS cm^{-1})**
P(CL-*co*-AVL)-**LD**-*g*-O3HT-**15**	49 ± 5.5	(2.86 ± 0.2.45) x 10^{-2}
P(CL-*co*-AVL)-**HD**-*g*-O3HT-**15**	52 ± 7.7	0.83 ± 0.07
P(CL-*co*-AVL)-**LD**-*g*-O3HT-**30**	60 ± 4.1	0.87 ± 0.35
P(CL-*co*-AVL)-**HD**-*g*-O3HT-**30**	47 ± 8.6	1.18 ± 0.41

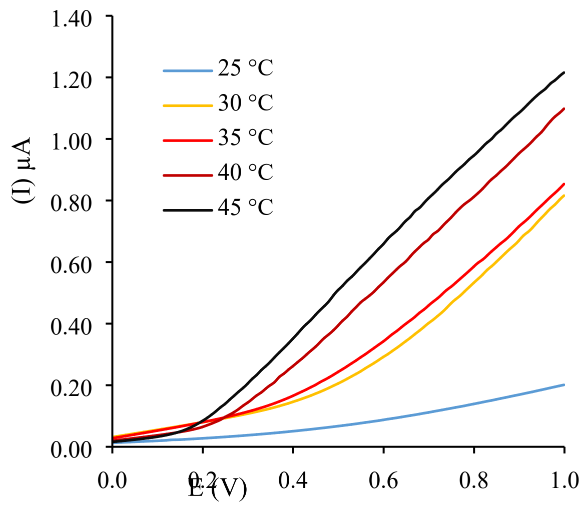

Figure S21. *I*-*V* curves (from 0 V to 1 V) of P(CL-*co*-AVL)-**HD**-*g*-O3HT-**30** at temperatures between room temperature (25 °C) and 45 °C.

Table S3: Temperature-dependent conductivities of the grafted P(CL-*co*-AVL)-**HD**-*g*-O3HT-30 calculated using the slopes from the linear parts of the curves in Figure S21.

Temperature, °C	Conductivity (mS cm^{-1})
25	0.02
30	0.85
35	0.89
40	0.93
45	1.00

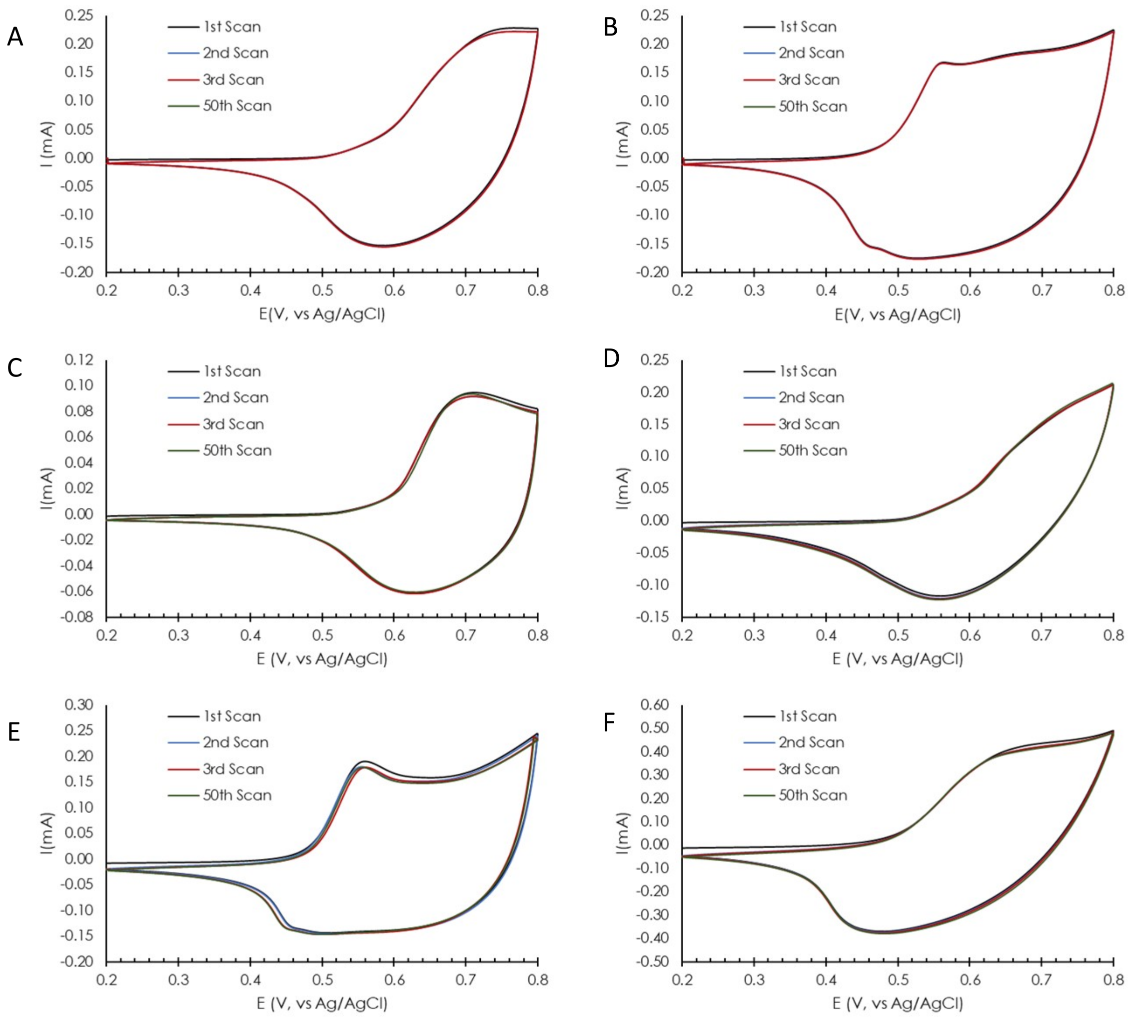

Figure S22: Cyclic Voltammograms of O3HT-**15** (A), O3HT-**30** (B), P(CL-*co*-AVL)-**LD**-*g*-O3HT-**15** (C), P(CL-*co*-AVL)-**HD**-*g*-O3HT-**15** (D), P(CL-*co*-AVL)-**LD**-*g*-O3HT-**30** (E) and P(CL-*co*-AVL)-**HD**-*g*-O3HT-**30** (F), cycled 50 cycles, with 1st, 2nd, 3rd and 50th scan shown.

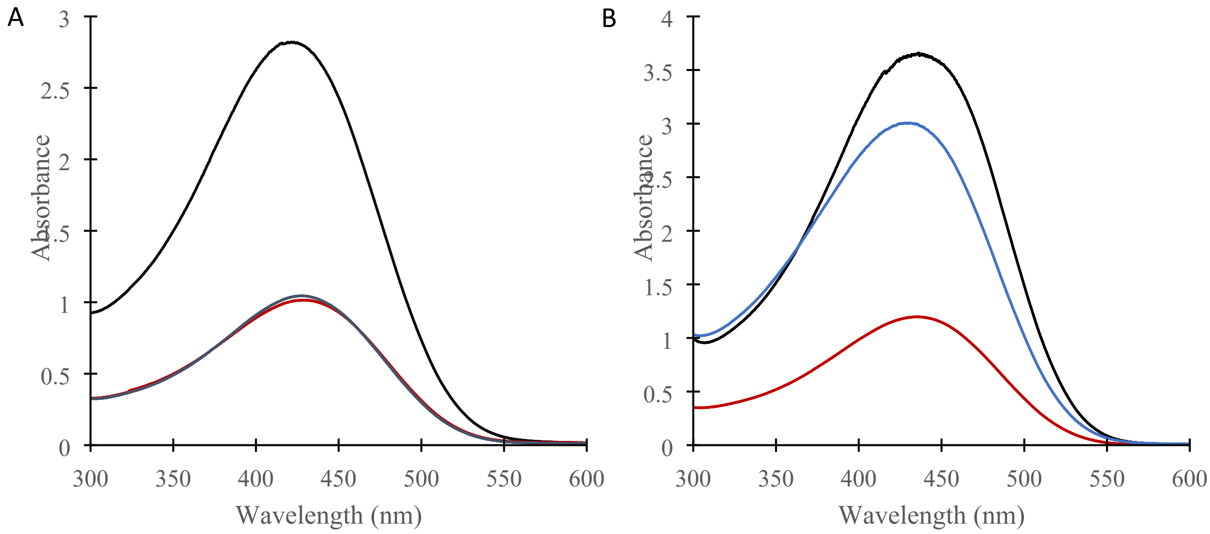

Figure S23: UV-Vis adsorption spectra of A) O3HT-**15** (black), P(CL-*co*-AVL)-**LD**-*g*-O3HT-**15** (red) and P(CL-*co*-AVL-**HD**-*g*-O3HT-**15** (blue) and B) O3HT-**30** (black), P(CL-*co*-AVL-**LD**-*g*-O3HT-**30** (red) and P(CL-*co*-AVL)-**HD**-*g*-O3HT-**30** (blue) in THF at 0.1 mg/mL.

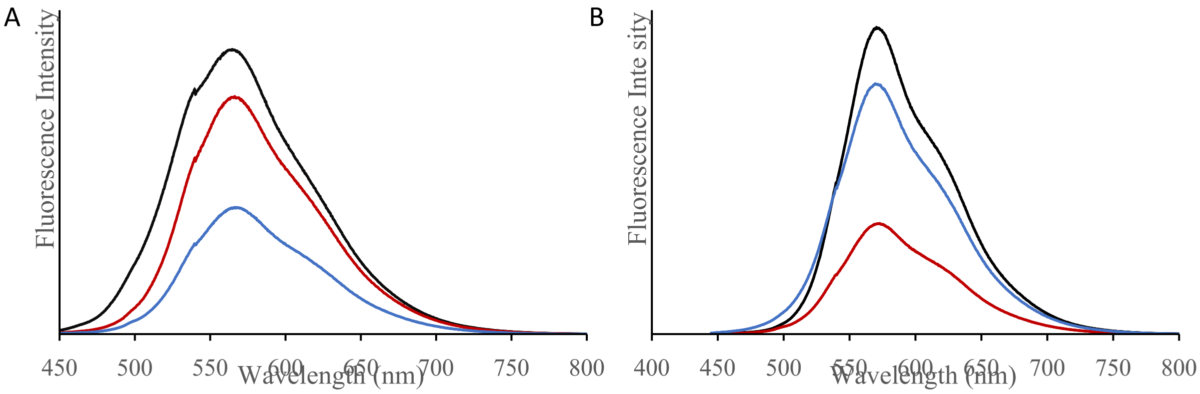

Figure S24: Fluorescence emission spectra of A) O3HT-**15** (black), P(CL-*co*-AVL)-**LD**-*g*-O3HT-**15** (red) and P(CL-*co*-AVL)-**HD**-*g*-O3HT-**15** (blue) and B) O3HT-**30** (black), P(CL-*co*-AVL)-**LD**-*g*-O3HT-**30** (red) and P(CL-*co*-AVL)-**HD**-*g*-O3HT-**15** (blue) in THF at 5 μg/mL.

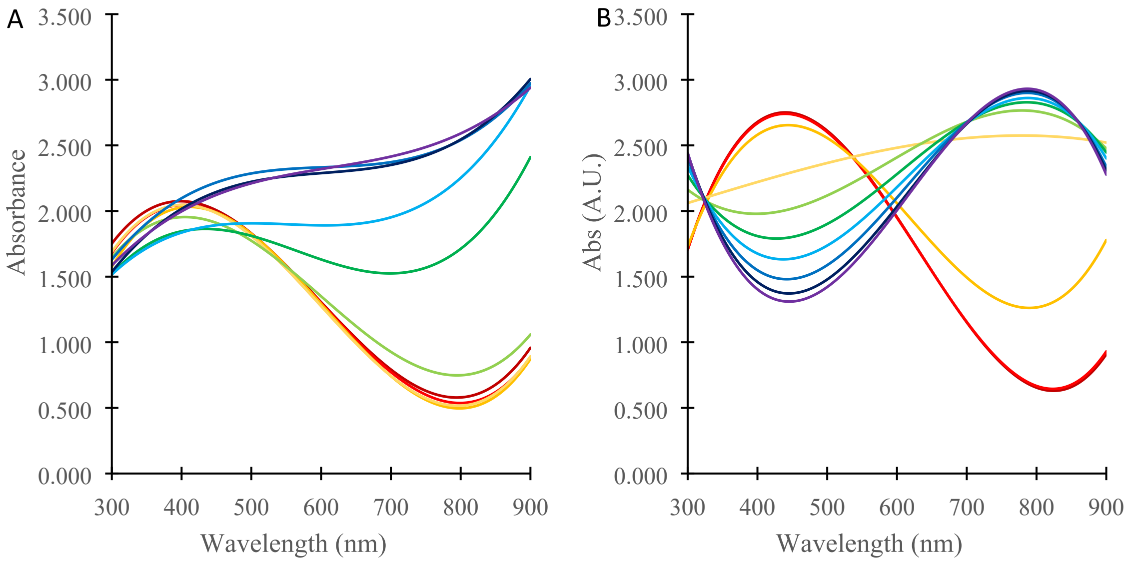

Figure S25: SEC spectra of O3HT-**15** (A) and O3HT-**30** (B) drop casted on ITO glass slides, between 0.1 V to 1.0 V, smoothed with 3rd Order Polynomial Fit.

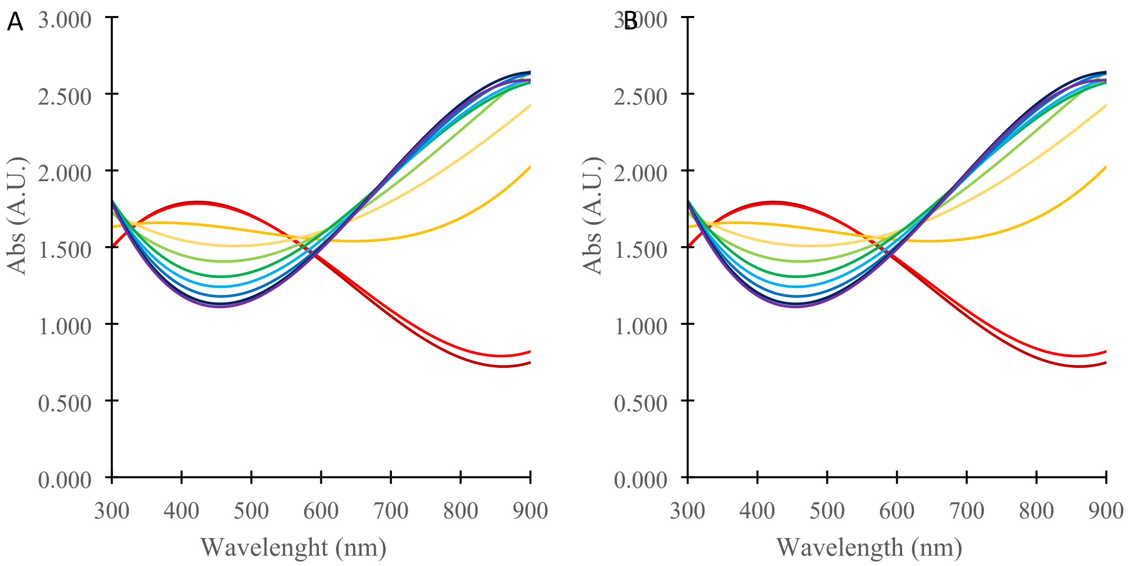

Figure S26: SEC spectra of P(CL-*co*-AVL)-**LD**-*g*-O3HT-**30** (A) and P(CL-*co*-AVL)-**HD**-*g*-O3HT-**30** (B) drop casted on ITO glass slides, between 0.1 V to 1.0 V, smoothed with 3rd Order Polynomial Fit.

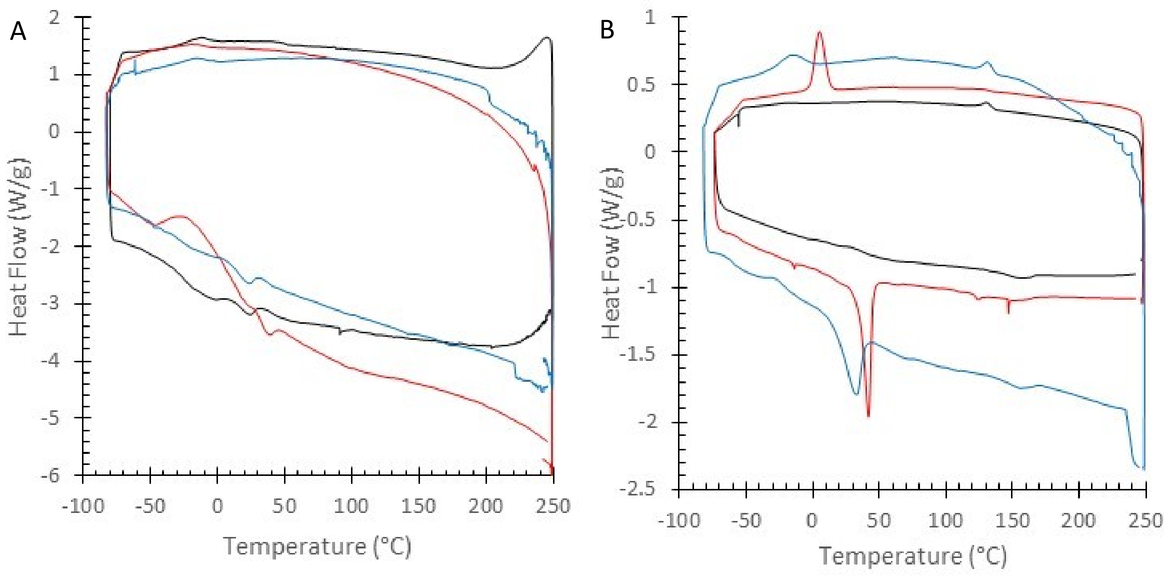

Figure S27: A) DSC curves of O3HT-**15**, P(CL-*co*-AVL)-**LD**-*g*-O3HT-**15** (red) and P(CL-*co*-AVL)-**HD**-*g*-O3HT-**15.** B) DSC curves of O3HT-**30**, P(CL-*co*-AVL)-**LD**-*g*-O3HT-**30** (red) and P(CL-*co*-AVL)-HD-*g*-O3HT-**30** (blue).

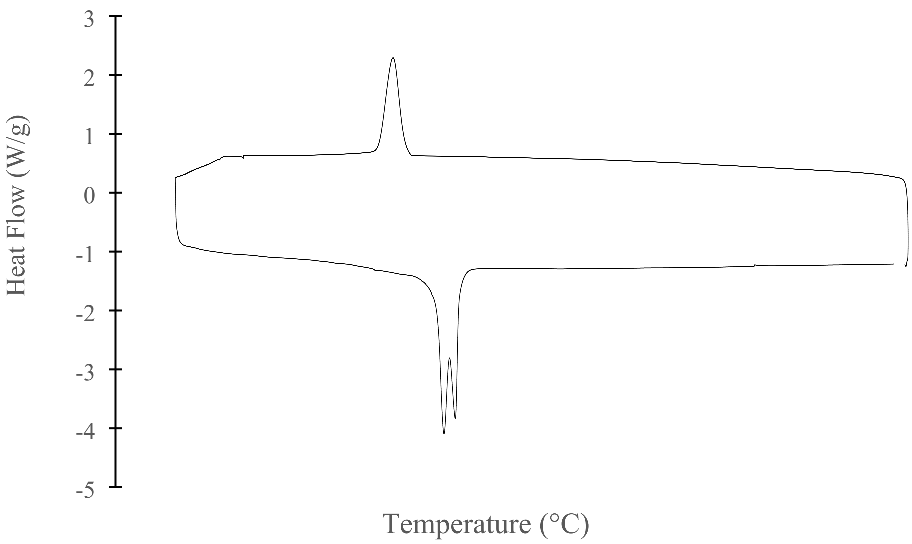

Figure S28: DSC scan of P(CL-*co*-AVL)-**LD**.

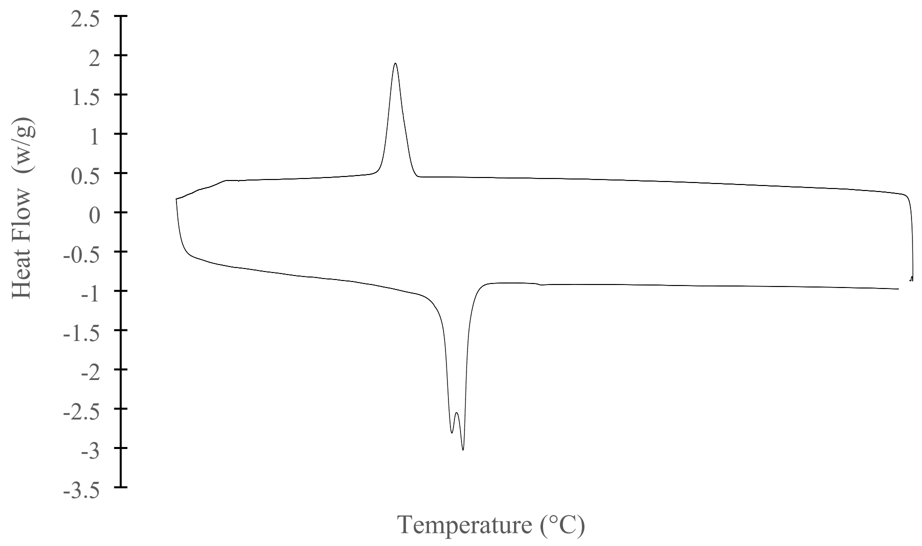

Figure S29: DSC scan of P(CL-*co*-AVL)-**HD**.

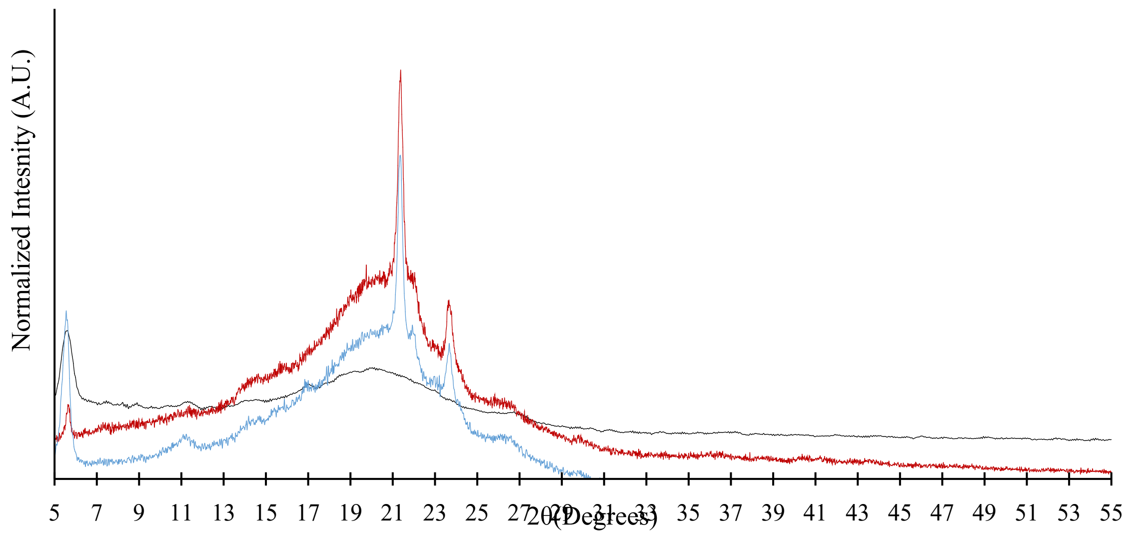

Figure S30: Normalized XRD spectra of O3HT-**15** (black), P(CL-*co*-AVL)-**LD**-*g*-O3HT-**15** (red) and P(CL-*co*-AVL)-**HD**-*g*-O3HT-**15** (blue)

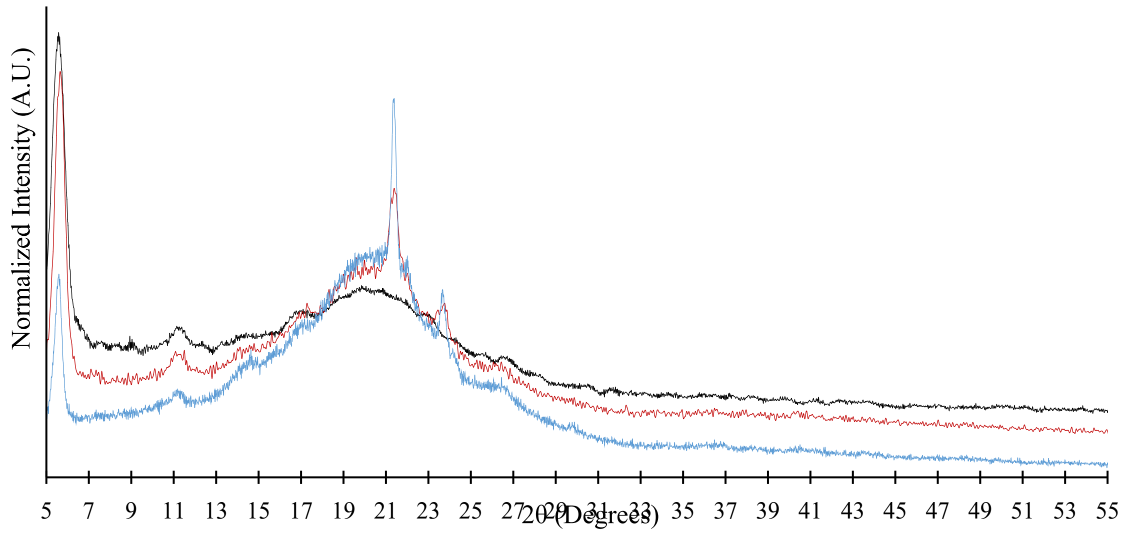

Figure S31: Normalized XRD spectra of O3HT-**30** (black), P(CL-*co*-AVL)-**LD**-*g*-O3HT-**30** (red) and P(CL-*co*-AVL)-**HD**-*g*-O3HT-**30**.

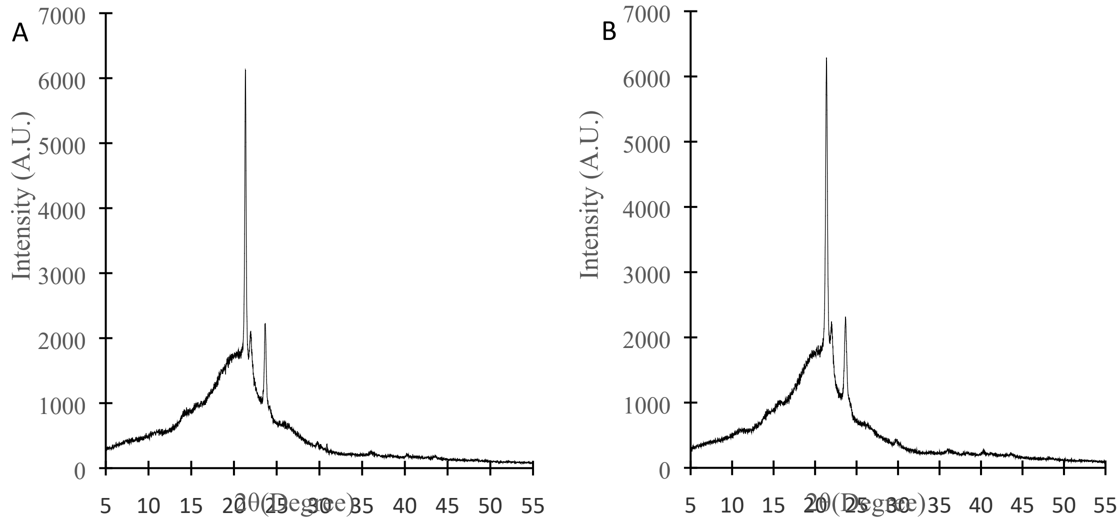

Figure S32: XRD spectra of (A) P(CL-*co*-AVL)-**HD** and (B) P(CL-*co*-AVL)-**LD**.

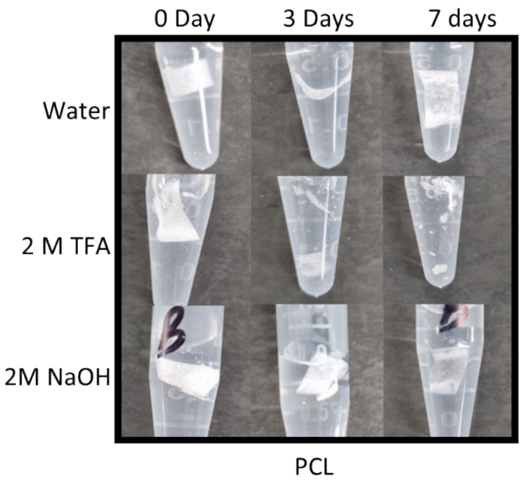

Figure S33: Optical photographs of PCL in water, 2 M TFA and 2 M NaOH at 0, 3 and 7 days.

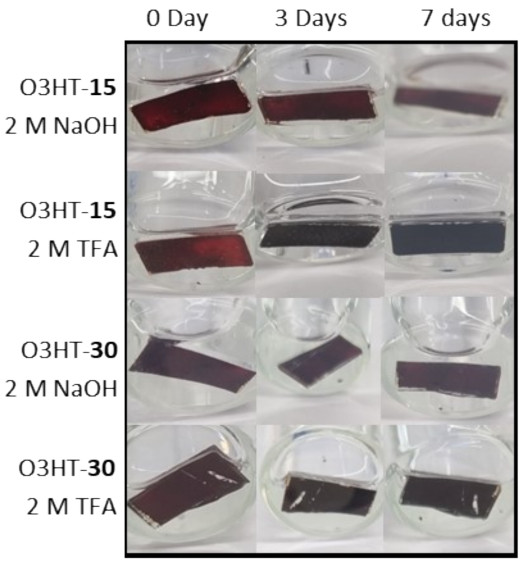

Figure S34: Optical photographs of O3HT-15 and O3HT-30 in 2 M TFA and 2 M NaOH at 0, 3 and 7 days.

Table S4. Conducting polymer-based transient electronic materials

Polymer		Electrical Properties	Degradation Method	Ref
P(CL-*co*-AVL)-*g*-O3HT	Degradable backbone	5.6 mS cm^{-1}	Acid, base and enzymatic degradation	This study
Gelatin-*graft*-poly(3-hexylthiophene)	Degradable backbone	$1.65 \pm 0.02 \times 10^{-7}$ S/cm	enzymatic degradation	1
PPy/PVDF (polyvinylidene fluoride)-based nanofibers	Composite	12 to 24 S/cm	Acetone dissolution	2
PPy/chitosan	Composite	1×10^{-2} S/cm	Lysozyme enzymatic degradation and *in vivo* degradation in rats	3
PEDOT:PSS/montmorillonite	Composite	8 to 16 S/cm	Ingestion by superworms	4
PEDOT/carboxymethyl chitosan	Composite	4.68×10^{-3} S/cm	Enzymatic degradation lysozyme	5
Oligoaniline-based electroactive blocks	Degradable backbone	8.34×10^{-8} S/cm	Enzymatic degradation	6
Quaterthiophene-*co*-adipic acid polyester (QAPE)	Degradable backbone	10^{-4} S/cm	Enzymatic degradation	7
Polyester organogels with aniline oligomers	Degradable backbone	1.03×10^{-5} S/cm	Acid hydrolysis	8,9
Poly(diketopyrrolopyrrole-phenylene diamine) (PDPP-PD)	Degradable semiconductor	Charge mobility 0.03 cm^2/V·s	Acid-meditated degradation	10,11
Poly(naphthalene diimide-*co*-(*E*,*E*)-N,N'1,4-phenylenebis[1-(2-thienyl)methanimine]) (PNDIT2/IM-*f)*	Degradable semiconductor	electron mobility (μe) 0.04 cm2 V^{-1} s^{-1}	Acid hydrolysis	12
Water-soluble transient conjugated polymer based on polypyrrole (PPY)	Soluble copolymer	Capacitance value 73 mF/g	Water soluble	13

References

1 X. Sun, E. W. C. Chan, Q. Chen, N. Kirby, J. Yang, J. P. Mata, R. L. Kingston, D. Barker, L. Domigan and J. Travas-Sejdic, *ACS Appl. Mater. Interfaces*, 2024, **16**, 23872–23884.
2 S. Veeralingam and S. Badhulika, *ACS Appl. Bio Mater.*, 2021, **4**, 14–23.
3 Y. Wan, A. Yu, H. Wu, Z. Wang and D. Wen, *J. Mater. Sci. Mater. Med.*, 2005, **16**, 1017–1028.
4 S. Lee, Y. Hong and B. S. Shim, *Adv. Sustain. Syst.*, 2022, **6**, 2100056.
5 C. Xu, S. Guan, S. Wang, W. Gong, T. Liu, X. Ma and C. Sun, *Mater. Sci. Eng. C*, 2018, **84**, 32–43.
6 J. G. Hardy, D. J. Mouser, N. Arroyo-Currás, S. Geissler, J. K. Chow, L. Nguy, J. M. Kim and C. E. Schmidt, *J. Mater. Chem. B*, 2014, **2**, 6809–6822.
7 N. K. E. Guimard, J. L. Sessler and C. E. Schmidt, *Macromolecules*, 2009, **42**, 502–511.
8 B. Guo, A. Finne-Wistrand and A.-C. Albertsson, *Macromolecules*, 2011, **44**, 5227–5236.
9 B. Guo, A. Finne-Wistrand and A.-C. Albertsson, *J. Polym. Sci. Part Polym. Chem.*, 2011, **49**, 2097–2105.
10 T. Lei, M. Guan, J. Liu, H.-C. Lin, R. Pfattner, L. Shaw, A. F. McGuire, T.-C. Huang, L. Shao, K.-T. Cheng, J. B.-H. Tok and Z. Bao, *Proc. Natl. Acad. Sci.*, 2017, **114**, 5107–5112.
11 H. Tran, V. R. Feig, K. Liu, H.-C. Wu, R. Chen, J. Xu, K. Deisseroth and Z. Bao, *ACS Cent. Sci.*, 2019, **5**, 1884–1891.
12 H. Park, Y. Kim, D. Kim, S. Lee, F. S. Kim and B. J. Kim, *Adv. Funct. Mater.*, 2022, **32**, 2106977.
13 J. Moon, V. Diaz, D. Patel, R. Underwood and R. Warren, *Org. Electron.*, 2022, **101**, 106412.